Available online at www.sciencedirect.com
ScienceDirect
Journal of Power Sources 174 (2007) 484–492
JOURNAL OF POWER SOURCES
www.elsevier.com/locate/jpowsour

Effects of anode active materials to the storage-capacity fading on commercial lithium-ion batteries

Gunho Kwak [a,*], Jounghwan Park [a], Jinuk Lee [a], Sinja Kim [b], Inho Jung [b]

[a] *Energy Business Division, Samsung SDI Co. Ltd., Sungsung-Dong, Cheonan-Si, Chungcheongnam-Do 330-300, South Korea*
[b] *Corporate R&D Center, Samsung SDI Co. Ltd., Sungsung-Dong, Cheonan-Si, Chungcheongnam-Do 330-300, South Korea*

Available online 29 June 2007

Abstract

Thermal storage of prismatic Li-ion cell with different types of anodes has been performed at 60 °C for 15 days to 30 days. The results were compared for two anodes: natural-like graphite (NLG) with styrene–butadiene rubber (SBR, 2.5 wt.%) binder and artificial graphite (AG) with polyvinylidene fluoride (PVdF, 6 wt.%) as binder. The storage-capacity fading behavior of the commercial Li-ion cell was studied by dissection the storage cells and analyzing their electrodes and solid electrolyte interphase (SEI), allows lithium-ion transfer but prevents electron migration using SEM, DSC, FT-IR, XRD and impedance analysis. Side-reaction and transformation of the passivation film on NLG anode contributed the capacity loss. Self-discharge of NLG cell due to high specific surface area was one of the main factors for capacity fading. Impedance analysis revealed that the interfacial resistance at NLG anode was larger than that of the AG anode. The increase of lithium alkylcarbonate and lithium carbonate due to reductive decomposition of electrolyte with storage time decreased the charge and increased the interfacial resistance.

Keywords: Lithium-ion battery; Storage-capacity fade; Natural-like graphite; Artificial graphite; Solid electrolyte interphase

1. Introduction

The new generations of mobile electronic devices require much more capacity and higher power since they will be operated with such modes as digital camera, multi-functional cell phone, network games, portable computers, hand-held power tools, and hybrid electric vehicles [1–5]. The power sources for mobile applications are requested not to be primary batteries but secondary batteries or fuel cells in view of economy, environment and materials savings. Among the various existing rechargeable batteries, lithium-based batteries appear to occupy a prime position in the energy density. New materials and technical developments are expected to help realize the goal of higher capacity to mobile electronic devices [6–11]. It is desirable to maintain the initial capacity of the battery with storage time. However, the capacity loss occurs in almost all the commercial rechargeable batteries. The mechanism of the capacity fading has not been completely understood, although some factors such as electrochemical reactions of electrolyte solution, irreversible phase and structure transition of active materials, and dissolution of cathode into the electrolyte concerned have been discussed [12–17]. Furthermore, capacity retention and storage life of the Li-ion cells deeply relate to the stability of the passivation layer. The control of the electrode/electrolyte interfaces is significant for high capacity and stable storage property of Li-ion rechargeable batteries in addition to the development of active materials and electrolytes. Especially, a major problem of the carbonaceous anode materials is their capacity loss during the cycle or the storage [18].

In this study, the high-temperature storage and the capacity fading of prismatic commercial Li-ion cells are investigated at various states of charge (SOC) with different anode active materials and binders. Natural-like graphite with styrene–butadiene rubber binder and artificial graphite with polyvinylidene fluoride as binder were used as anode active materials for investigation of the storage-capacity fading phenomenon on commercial Li-ion batteries, respectively.

2. Experimental

The prismatic Li-ion batteries were chosen as samples from commercially available batteries with different anode materi-

* Corresponding author. Tel.: +82 10 9347 4629; fax: +82 41 560 3696.
E-mail address: gh.kwak@samsung.com (G. Kwak).

0378-7753/$ – see front matter © 2007 Elsevier B.V. All rights reserved.
doi:10.1016/j.jpowsour.2007.06.169

als (NLG and AG) but same cathode material ($LiCoO_2$). The nominal capacities were 1130 mAh (NLG) and 780 mAh (AG), respectively. The electrolytes were based on organic carbonates such as ethylene carbonate (EC), propylene carbonate (PC), dimethyl carbonate (DMC), and diethyl carbonate (DEC) with 1.15 M $LiPF_6$.

All the samples for the analysis were treated in the glove box under the control of $H_2O < 1$ ppm and $O_2 < 1$ ppm by helium. The samples, which containing the electrolyte, were treated carefully using purified DMC in the dry glove box. For the observation of surface morphology of the negative electrode, we used two different types of scanning electron micrograph (SEM; Philips, XL-30 and Zeol, JSM6340F). Differential scanning calorimetry (DSC; TA, 2910) was used to measure the change of the thermal properties for the SEI formed on anode electrode and for the reaction of oxidation caused by O_2 generation from cathode material. The heating rate was 10 °C min^{-1} in the range from 25 °C to 300 °C. To investigate the component of the SEI layer, we decided to characterize FT-IR spectrometer (Nicolet, NEXUS-8700/Continum). To confirm the influence of the self-discharge through the change of Li content of the graphite anode material, we selected X-ray diffractometer (XRD, Bruker, D8 discover). Impedance analysis for the internal and interfacial properties of storage cells was performed at room temperature using an ac impedance analyzer (IM6, Zhaner) in the frequency range from 50Hz to 1 MHz.

3. Results and discussion

Figs. 1 and 2 show retention and recovery capacity as a function of storage time and SOC. Retention curves indicate not only a voltage drop but also capacity loss with the time. It reveals that the SOC and the type of anode active materials play an important role to capacity fading effect in this system. The recovery capac-

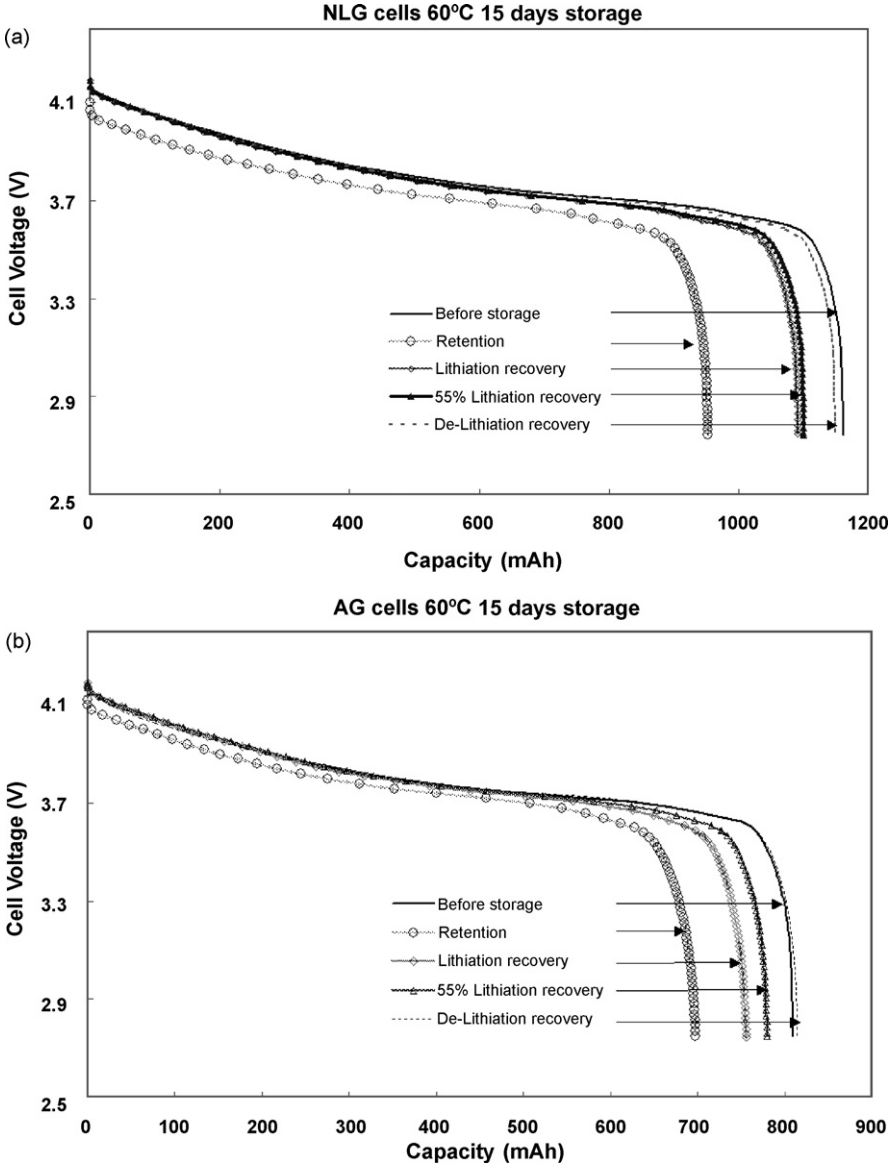

Fig. 1. Capacity profiles before and after 15 day-storage cells with different states of charge: (a) NLG and (b) AG.

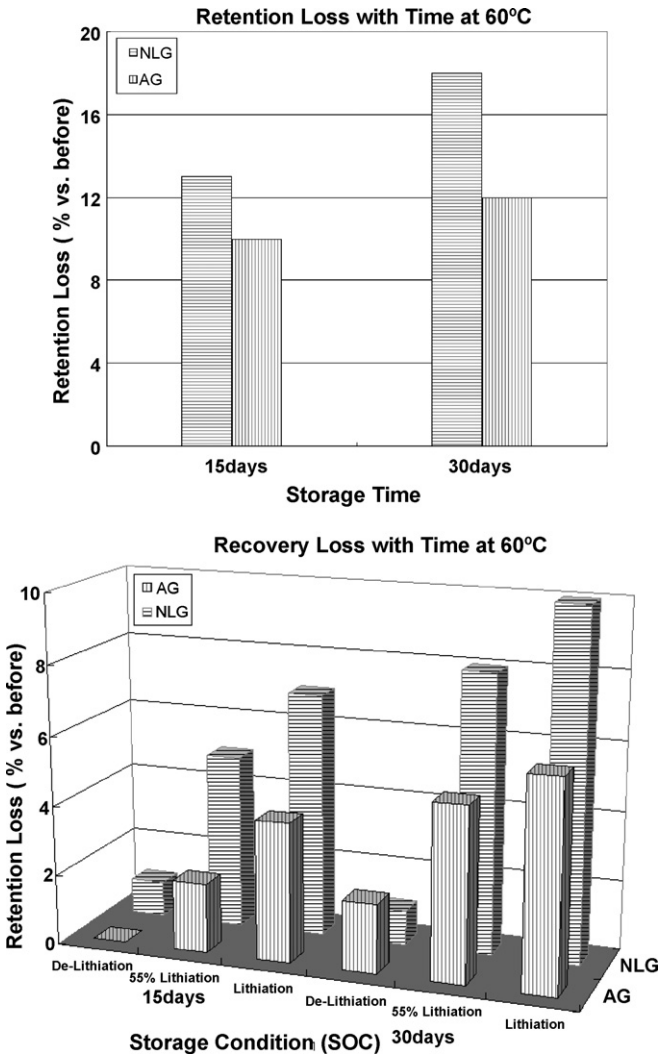

Fig. 2. Retention and recovery loss of storage cells with SOC and storage time.

Table 1
Comparison of the physical properties and the electrochemical performance of NLG and AG at room temperature

	Natural-like graphite (NLG)	Artificial graphite (AG)	Remarks
Capacity	~540 mAh cm^{-3} ~360 mAh g^{-1}	~510 mAh cm^{-3} ~340 mAh g^{-1}	– –
Efficiency	~93%	~95%	–
Capacity	~320 mAh g^{-1}	~300 mAh g^{-1}	1 C-rate
Cycle life	~85%	85% ↑	At 300 cycle
Shape	Massive, flaky	Spherical, fibril	–
Lattice coefficient	~3.360 Å	~3.365 Å	d_{002}
Specific surface area	~5 m^2 g^{-1}	~2 m^2 g^{-1}	–
Binder	SBR/CMC/H_2O	PVdF/NMP	–
Characteristic	Non-crystalline Low adhesive strength High capacity Environmentally benign	Crystalline High adhesive strength High fluidity NMP treatment	–

ity of the storage cells with de-lithiation shows almost same capacity with the fresh cells. The charge consumption increases with increasing the storage time for the both cells. However, the capacity loss of the NLG is larger than that of the AG. As shown in Table 1, it supposes that the high specific surface area and the different shapes of NLG could influence the capacity fading of the battery. It also presents high internal resistance with time compared to AG system shown in Figs. 3 and 4. To measure the ratio of Li intercalation in anode with storage time X-ray diffraction study was done for fresh as well as thermal storage anode materials. Fig. 5(a) shows the XRD pattern of the 55% lithiated NLG anode. From the relative peak area, we derived an experimental equation to calculate the lithiation ratio in anode

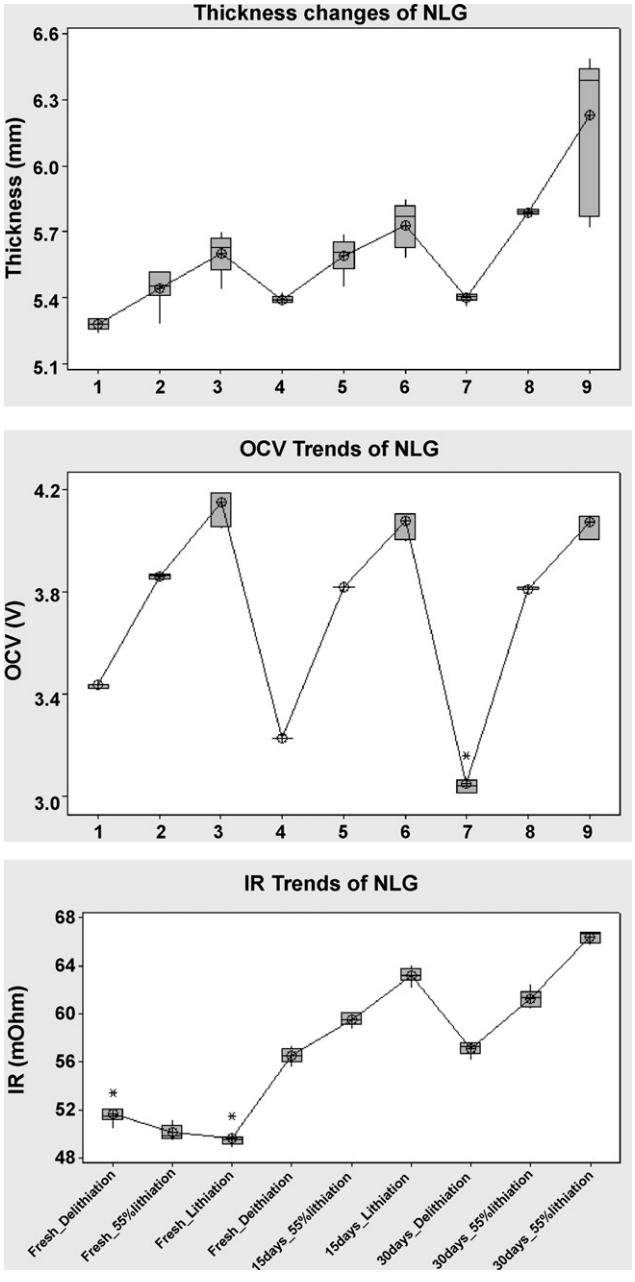

Fig. 3. Variation of cell thickness, OCV, and IR for NLG cells.

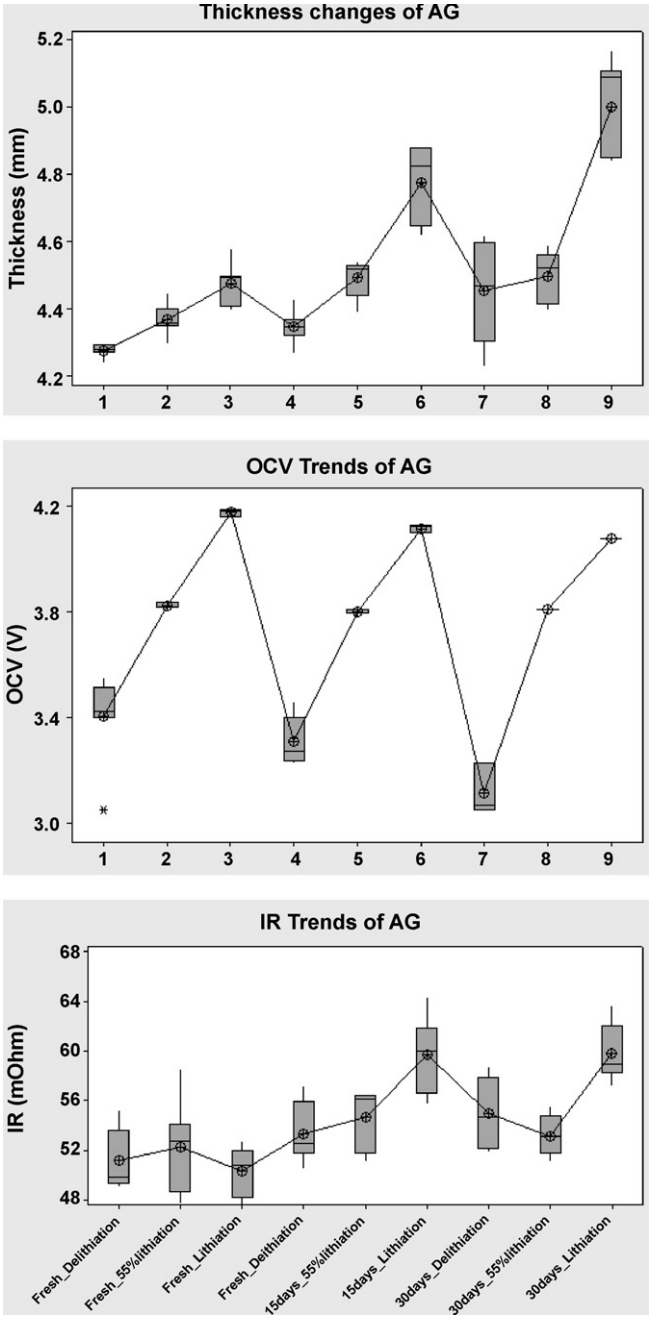

Fig. 4. Variation of cell thickness, OCV, and IR for AG cells.

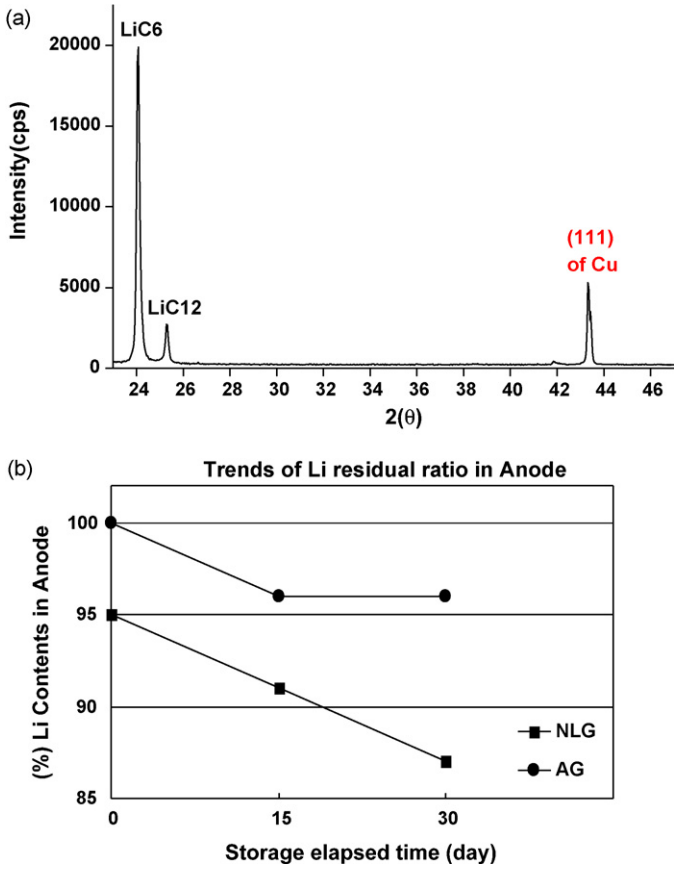

Fig. 5. X-ray diffractometer of NLG fresh cell (a) and lithium residual ratio in anode with storage time (b).

with storage time

$$\text{Lithiation ratio in anode} = \frac{\text{LiC}_6}{\text{LiC}_6 + \text{LiC}_{12}} \times 1.0 + \frac{\text{LiC}_{12}}{\text{LiC}_6 + \text{LiC}_{12}} \times 0.5 \quad (1)$$

It is originated from the relative peak area between the LiC_6 of lithiation and the LiC_{12} of 55% lithiation cells. It provides a reasonable result about the residual Li content in graphite. As shown in Fig. 5(b), AG cell preserves 95% of Li content after 30 days but NLG cell shows linear decrease of Li content with storage time. It shows a strong presumption for self-discharge of Li from the NLG electrode and reveals a good agreement with the capacity trends mentioned in Figs. 1 and 2.

Changes in electrode interface with storage time were studied carefully by inspection of scanning electron micrographs of the electrode surface in order to obtain additional clues as to why the NLG cells lose their capacity with storage time. Figs. 6 and 7 present the surface morphology of disassembled anode electrode. NLG cells show large and harsh deformed area compared to AG cells. It is presumed that the higher capacity fade for the NLG storage cells at 60 °C was due to a repeated film formation over the interface of anode resulted in increased rate of Li consumption. It is thought that the deformed part of the NLG surface is caused by the side-reaction of electrolyte and thermally activated characteristic of NLG to increase the Li alkylcarbonate and Li carbonate during the high-temperature storage. FT-IR spectra provide a good evidence for the assumption in Fig. 8. The spectrum of a typical anode passivation film composed of Li alkylcarbonate and Li carbonate has been increased with storage time. We can verify the thickened layer visually using the SEM as Figs. 9 and 10. The layer is responsible for an irreversible capacity loss. However it protects against co-intercalation of solvent into the graphite and reduces an exfoliation of the graphite sur-

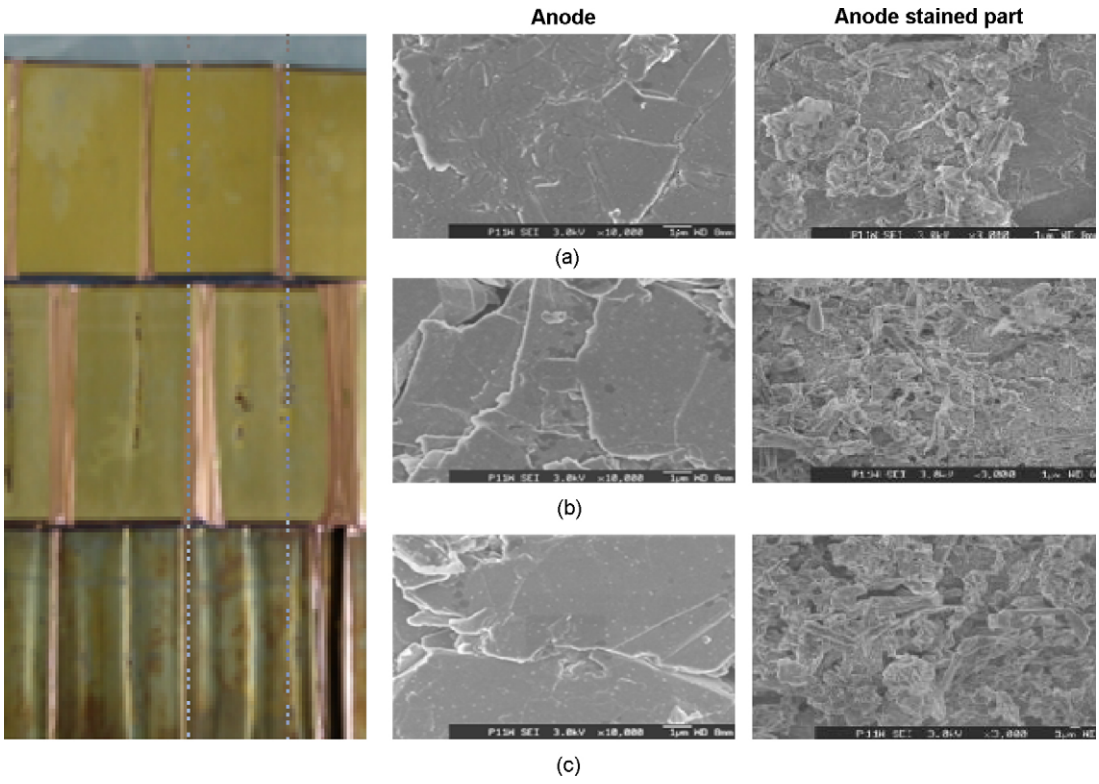

Fig. 6. Scanning electron micrographs of NLG anode after storage: (a) fresh, (b) 15 days, and (c) 30 days.

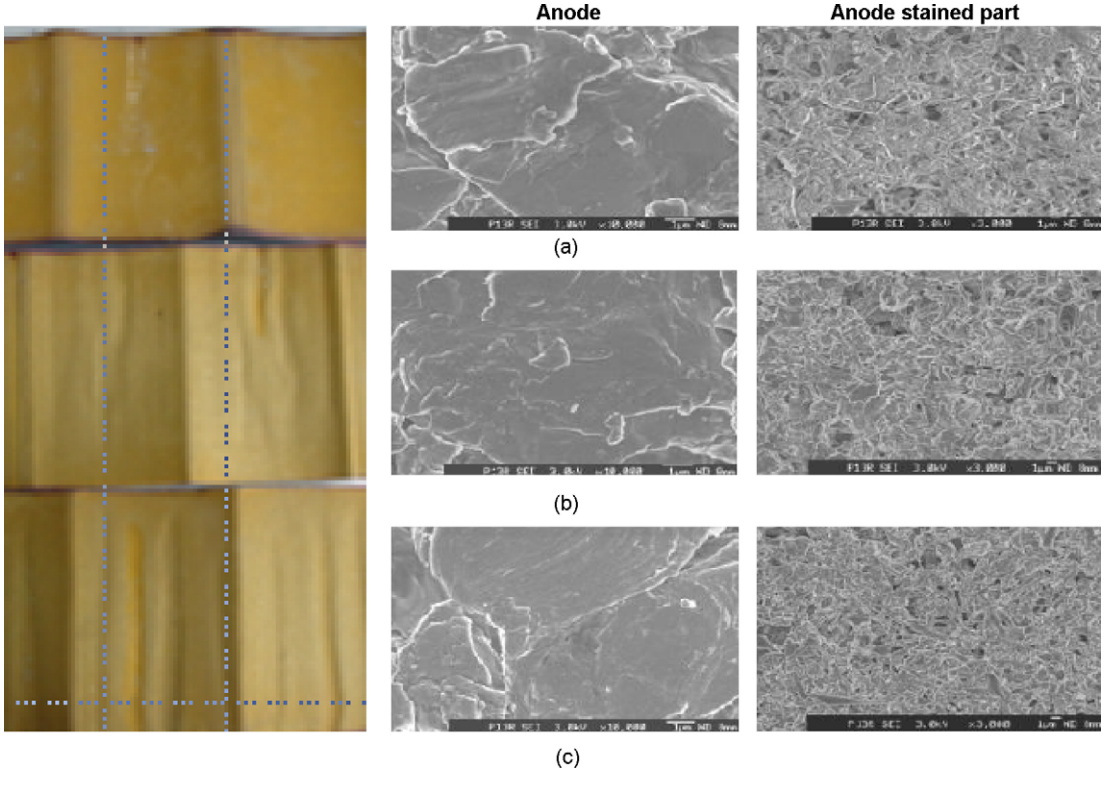

Fig. 7. Scanning electron micrographs of AG anode after storage: (a) fresh, (b) 15 days, and (c) 30 days.

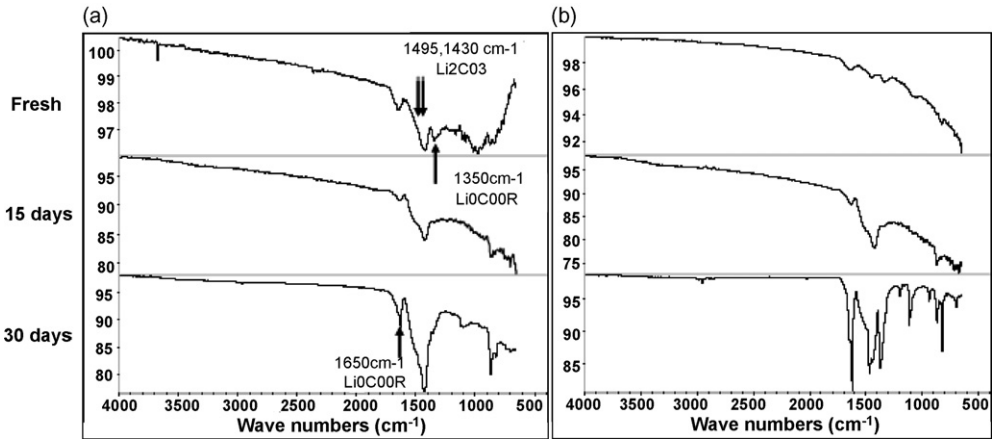

Fig. 8. FT-IR study of anode passivation film with storage time: (a) AG and (b) NLG.

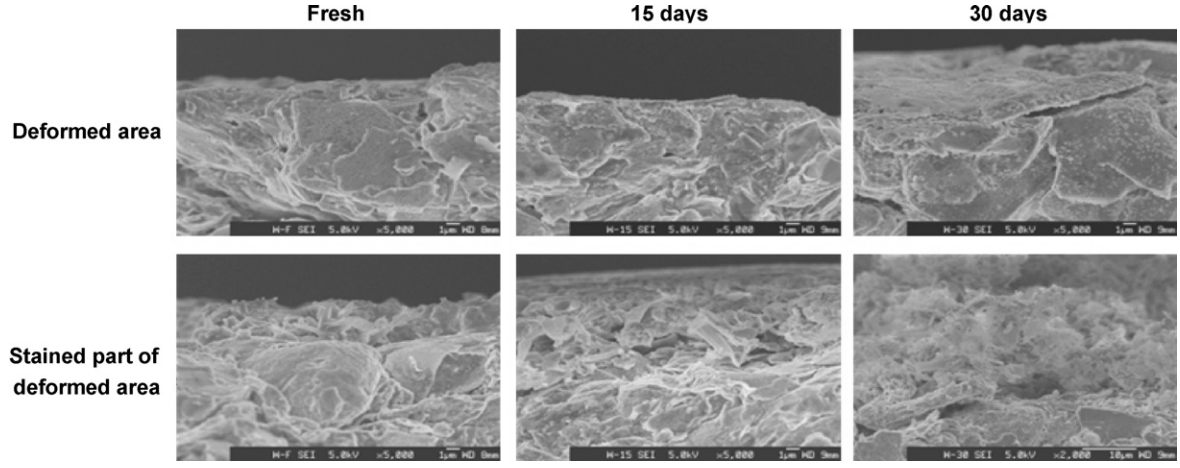

Fig. 9. Analysis of SEI formed on anode electrode for NLG cells with storage time.

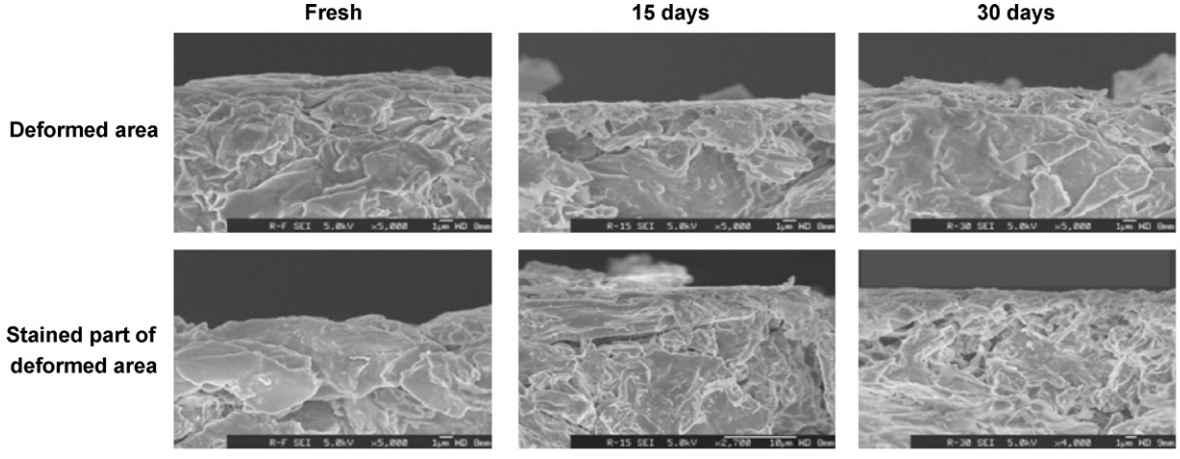

Fig. 10. Analysis of SEI formed on anode electrode for AG cells with storage time.

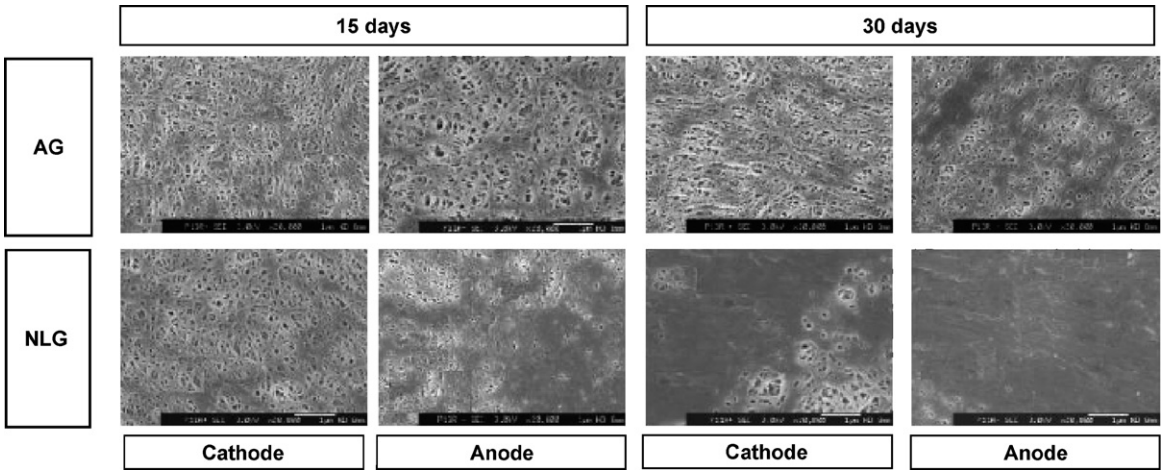

Fig. 11. Scanning electron micrographs of separators after storage.

face. From the figures we can confirm the by-product, which resulted from the side-reaction between self-discharged Li and electrolyte. As shown in Fig. 9 the by-product layer increased with storage time. However AG shows almost same shape and stable passivation layers (Fig. 10). It shows good coincidence with the retention capacity in this system. Fig. 11 presents the congestion of porosity on separator with storage time. It is considered that the by-product caused by the side-reaction contaminates the separators and is accumulated on the surface, which resulted in poor Li transfer and increased internal resistance.

The influence of the storage time on the thermal behavior has been determined from DSC measurements in Fig. 12. The onset temperature for thermal breakdown seems to be almost same of cathode. But the exothermic peaks of NLG anode shift to the higher temperature area with storage time, which may be explained by differences in surface structures, porosity, particle size and transformation of passivation film. It is shown that an impedance spectroscopy can give specified information about the state and the phenomenon inside a battery. The Nyquist plots of prismatic commercial Li-ion batteries were measured at various states of charge before and after the storage. As shown in Figs. 13 and 14, the plots show different behaviors with the anode type and the SOC. The inductive tail attributes to the jellyroll and porous active materials at high frequency followed by two loops at lower frequencies. It is assigned that the left loop at high frequencies in the Nyquist plot to the anode and the larger loop at low frequencies to the cathode. Furthermore, the values of R_{SEI} with storage time are smaller than those of NLG, meaning that the stable SEI of AG improves the permeation of Li-ion in the SEI film. It shows that the film resistance and the irreversible capacity are decreased in the case of AG-introduced battery system. The increase of the R_{SOL} and the R_{SEI} originates from the by-product due to unwanted side-reaction on the SEI/graphite interface. It interrupts the intercalation of lithium into graphite electrode. As experimental results, the capacity fade is also accompanied by an increase the interfacial resistance of the battery upon storage.

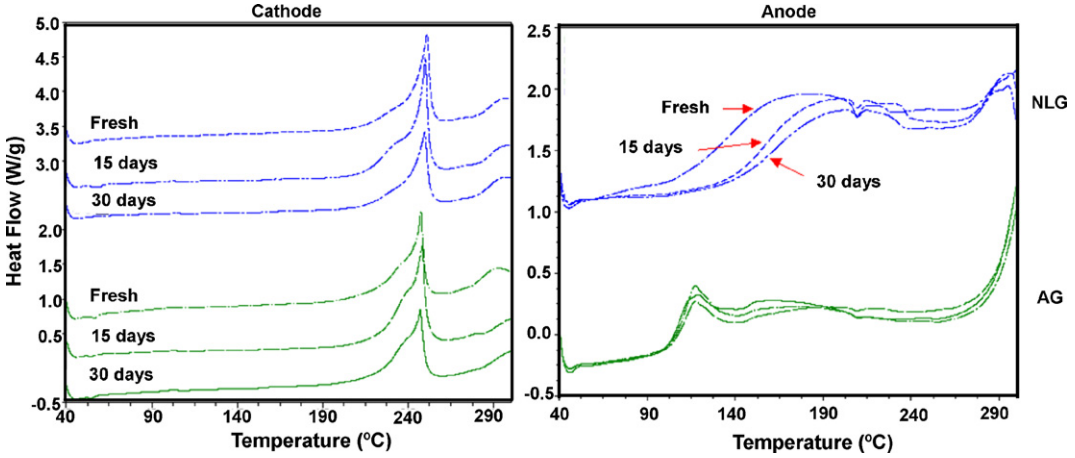

Fig. 12. DSC curves of the electrodes with storage time.

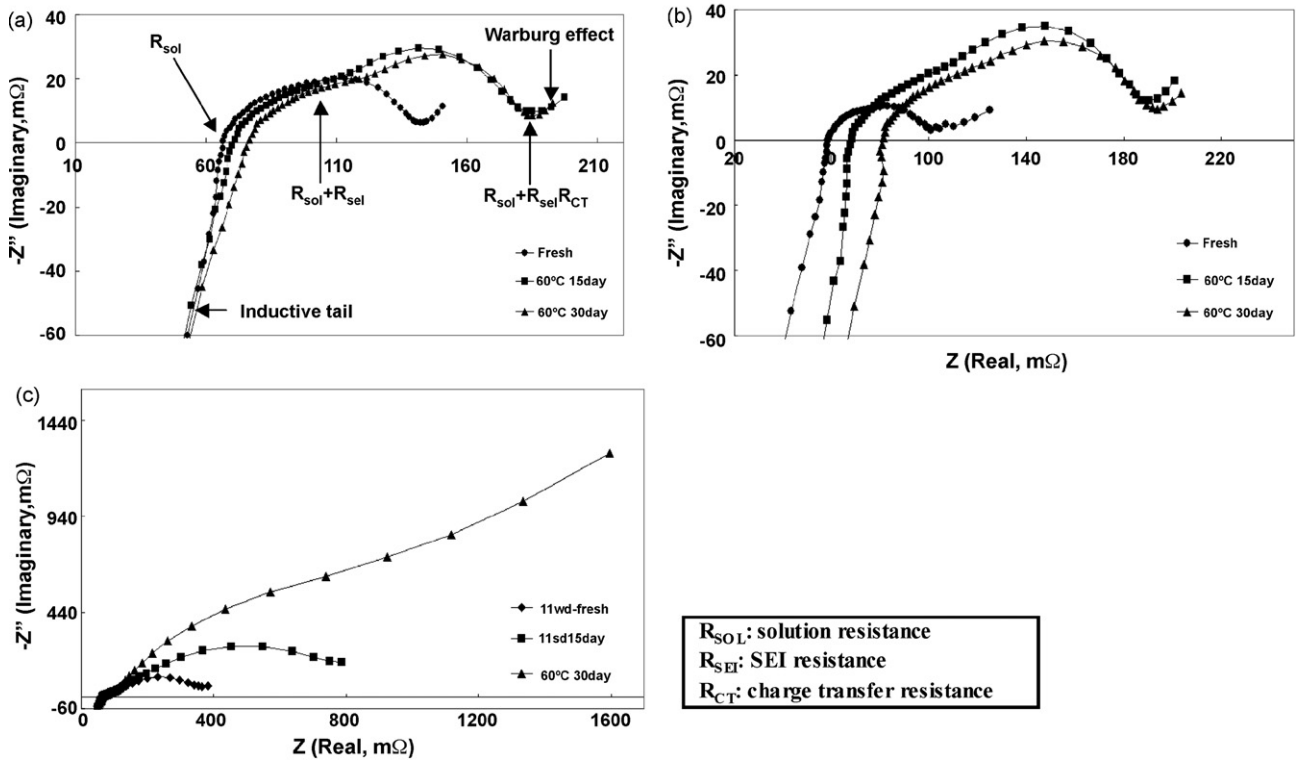

Fig. 13. Nyquist plots of the NLG cells with storage condition and time: (a) lithiation, (b) 55% lithiation, and (c) de-lithiation.

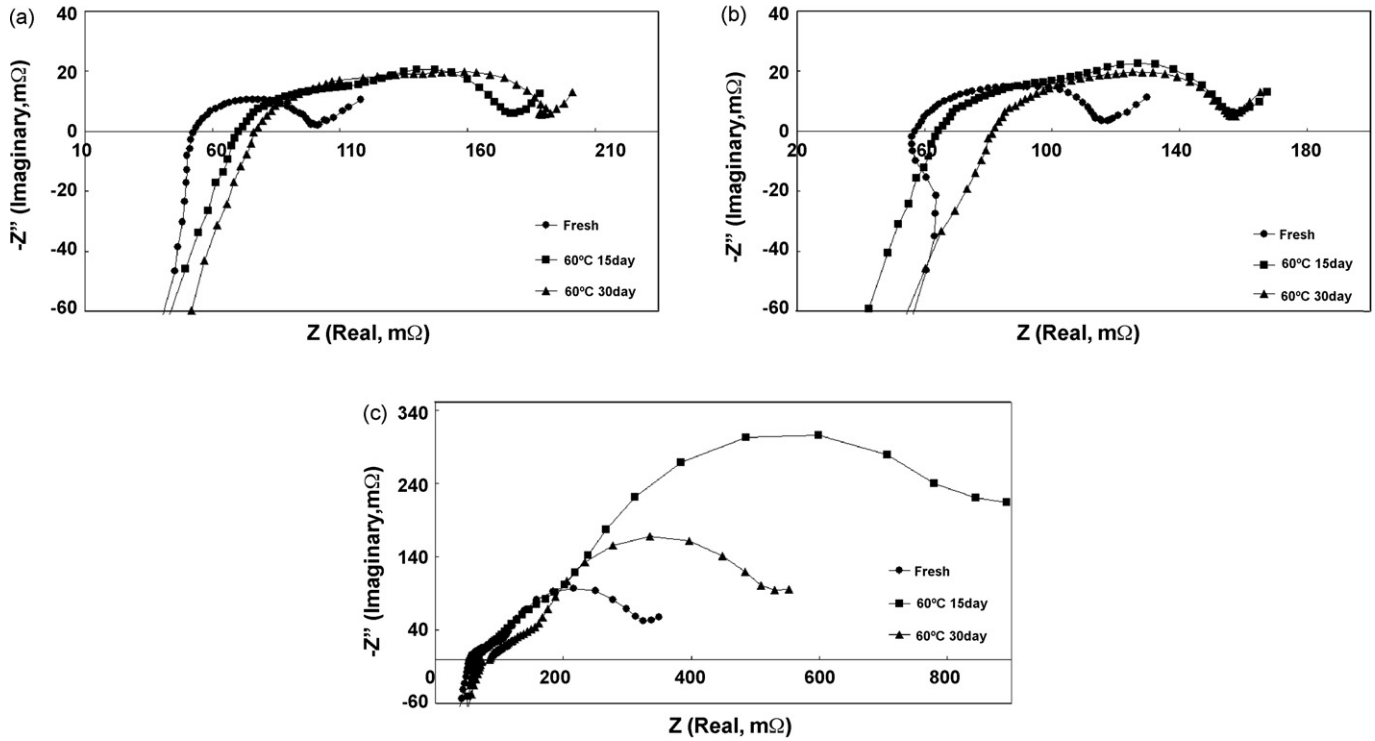

Fig. 14. Nyquist plots of the AG cells with storage condition and time: (a) lithiation, (b) 55% lithiation, and (c) de-lithiation.

4. Conclusions

The main purpose of this study was to investigate the influence of carbon type and structure on storage-capacity fade for the commercial prismatic Li-ion battery. An effective capacity fade analysis was carried out for commercial prismatic-type Li-ion cells stored at 60 °C. SEM, DSC, FT-IR, XRD and impedance analysis were carried out. The increased capacity loss for the cells stored at 60 °C can be explained by the side-reaction of electrolyte and the transformation of the passivation film over the surface of anode, which resulted in the increased Li-ion consumption and also in the cell resistance with storage time.

References

[1] C.A. Vincent, B. Scrosati, Modern Batteries: An Introduction to Electrochemical Power Sources, 2nd ed., John Wiley & Sons, New York, 1997.
[2] H.R. Allcock, C.R. Denus, R. Prange, W.R. Laredo, Macromolecules 34 (2001) 2757.
[3] F. Putois, H. Horie, J. Power Sources 57 (1995) 67.
[4] K.M. Abraham, M. Alamgir, J. Electrochem. Soc. 137 (1990) 1657–1658.
[5] G. Kwak, Y. Tominaga, S. Asai, M. Sumita, Electrochim. Acta 48 (2003) 1991.
[6] H.R. Allcock, W.R. Laredo, R.V. Morford, Solid State Ionics 139 (2001) 27.
[7] G. Kwak, Y. Tominaga, S. Asai, M. Sumita, Electrochim. Acta 48 (2003) 4069.
[8] M. Broussely, G. Archdale, J. Power Sources 136 (2004) 386.
[9] J. Fan, P.S. Fedkiw, J. Power Sources 72 (1998) 165.
[10] R. Spotnitz, J. Power Sources 113 (2003) 72.
[11] A. DuPasquier, P.C. Warren, D. Culver, A.S. Gozdz, G.G. Amatucci, J.M. Tarascon, Solid State Ionics 135 (2000) 249.
[12] P. Arora, R.E. White, M. Doyle, J. Electrochem. Soc. 145 (1998) 3647.
[13] M. Wohlfahrt-Mehrens, C. Vogler, J. Garche, J. Power Sources 127 (2004) 58.
[14] Y. Xia, M. Yoshio, J. Electrochem. Soc. 143 (1996) 825.
[15] S. Komaba, N. Kumagai, T. Sasaki, Y. Miki, Electrochemistry 69 (2001) 784.
[16] S. Megahed, B. Scrosati, J. Power Sources 76 (1994) 79.
[17] G. Nagasubramanian, J. Power Sources 87 (2000) 226.
[18] P. Ramadass, B. Haran, R. White, B.N. Popov, J. Power Sources 112 (2002) 614.